Determination of Particle Sources for a Geotail Distribution Function Observed on May 23, 1995

M. Ashour-Abdalla[1], M. El-Alaoui[1], V. Peroomian[1], J. Raeder[1], R. L. Richard[1], R. J. Walker[1], L. M. Zelenyi[2], L. A. Frank[3], W. R. Paterson[3], J. M. Bosqued[4], R. P. Lepping[5], K. Ogilvie[5], S. Kokubun[6], and T. Yamamoto[7]

On May 23, 1995, the Comprehensive Plasma Instrumentation (CPI) onboard the Geotail spacecraft observed a complex and structured ion distribution function near the magnetotail midplane at $x \sim -10\ R_E$. On the same day, the Wind spacecraft observed a very high density (~ 40 cm^{-3}) solar wind and an interplanetary magnetic field (IMF) that was predominantly northward but had several southward turnings. We have inferred the sources of the ions in this distribution function by following approximately 90,000 ion trajectories backward in time using time-dependent electric and magnetic fields obtained from a global MHD simulation. Wind data were used as input for the MHD model. We found that three sources contributed to this distribution: the ionosphere, the plasma mantle which had near-Earth and distant tail components, and the low latitude boundary layer (LLBL). Moreover, distinct structures in the low energy part of the distribution function were found to be associated with individual sources. Structures near 0° pitch angle were made up of either ionospheric or plasma mantle ions, while structures near 90° pitch angle were dominated by ions from the LLBL source. Particles that underwent nonadiabatic acceleration were numerous in the higher energy part of the ion distribution function, whereas ionospheric and LLBL ions were mostly adiabatic. A large proportion of the near-Earth mantle ions underwent adiabatic acceleration, while most of the distant mantle ions experienced nonadiabatic acceleration.

[1]Institute of Geophysics and Planetary Physics, University of California, Los Angeles, California
[2]Space Research Institute, Russian Academy of Sciences, Moscow, Russia
[3]Department of Physics and Astronomy, The University of Iowa, Iowa City, Iowa
[4]Centre d' Etude Spatiale des Rayonnements, CNRS, Toulouse, France
[5]NASA/Goddard Space Flight Center, Greenbelt, Maryland
[6]STELAB, Nagoya University, Toyokawa, Aichi, Japan
[7]ISAS, Sagamihara, Kanagawa, Japan

Geospace Mass and Energy Flow: Results From the International Solar-Terrestrial Physics Program
Geophysical Monograph 104

1. INTRODUCTION

A fundamental issue of magnetospheric physics is determining the origin of magnetospheric plasma (see review by *Hill* [1974]). Early investigations considered likely plasma sources to be solar wind plasma diffusing across the magnetopause [*Eastman and Hones*, 1979] and the polar wind. Observations revealed a layer of enhanced density adjacent to the magnetopause, which was termed the low latitude boundary layer (LLBL); the properties of this region indicated that it was a site of solar wind mass, momentum and energy transfer to the magnetosphere [*Hones et al.*, 1972a; *Eastman et al.*, 1976]. *Hones et al.* [1972b] also identified another potential source, the high latitude plasma mantle. *Pilipp and*

Morfill [1978] postulated that the mantle source could supply all of the plasma observed in the magnetotail. The plasma mantle and the LLBL are likely entry points for solar wind plasma. The first indication that ions of terrestrial origin could also constitute a substantial component of the energetic ion population in the magnetosphere was given by ion composition measurements [*Shelley et al.*, 1972] which showed fluxes of O^+, evidently of ionospheric origin, to be more common than H^+ fluxes during magnetic storms. Because there is a negligible amount of O^+ in the solar wind, this component was used as a tracer of ionospheric plasma. Since then, composition measurements from different satellites have established the presence of substantial O^+ fluxes everywhere in the magnetosphere at various times [*Geiss et al.*, 1978; *Lennartsson et al.*, 1979, 1981; *Lundin et al.*, 1980; *Balsiger et al.*, 1980; *Sharp et al.*, 1981]. Exactly how the ions reach a given region of the magnetotail from a plasma source, as well as the precise locations of the source regions, remains an open question.

Numerous studies have investigated plasma transport through the magnetotail; these include studies of ion beam acceleration and velocity dispersion in the plasma sheet boundary layer (PSBL) [*Jaeger and Speiser*, 1974; *Cowley*, 1980; *Williams*, 1981; *Green and Horwitz*, 1986; *Schindler and Birn*, 1987; *Curran and Goertz*, 1989], processes occurring near magnetic x-lines [*Speiser*, 1965; *Amano and Tsuda*, 1978; *Wagner et al.*, 1981; *Martin*, 1986; *Martin and Speiser*, 1988; *Savenkov et al.*, 1991], and studies of ion dynamics when there is a normal component of the magnetic field that is constant or slowly varying downtail [*Lyons and Speiser*, 1982; *Zelenyi et al.*, 1988; *Büchner and Zelenyi*, 1989]. A major result of particle trajectory studies was a recognition of the importance of the chaotic nature of ions [*Büchner and Zelenyi*, 1986, 1989; *Chen and Palmadesso*, 1986]. These studies used idealized electric and magnetic field models to show that particles could experience nonadiabatic acceleration in regions of highly curved magnetic field lines. *Ashour-Abdalla et al.* [1993] developed large-scale kinetics (LSK) in which the trajectories of a large number of noninteracting ions were calculated in model magnetic and electric fields to investigate the importance of nonadiabatic motion in determining the magnetotail plasma population. By using a uniform electric field and a 2D reduction of the *Tsyganenko* [1989] magnetic field model, they showed that the magnetotail could be populated from a plasma mantle source [*Ashour-Abdalla et al.*, 1993]. Moreover, they found that highly structured magnetotail ion distributions could result from nonadiabatic ion behavior [*Ashour-Abdalla et al.*, 1994, 1995]. A comparison of LSK distribution functions with those measured by the Galileo spacecraft showed substantial qualitative agreement between the observed and calculated distribution functions [*Ashour-Abdalla et al.*, 1993].

The Geotail spacecraft has given us new insight into the plasma distributions in the magnetotail. The advanced Geotail instruments allow a full 3-D coverage of velocity space with high time resolution. The detailed velocity distribution functions reveal puzzling details: bumps, beams and holes which presumably are signatures of the ions' histories. In data collected from the distant tail, *Frank et al.* [1996] observed nongyrotropic distribution functions near the equatorial current sheet. Closer to Earth, the ion distribution functions were complex and anisotropic, containing small-scale structures which *Frank et al.* [1996] attributed to the particles' "memory" of remote tail acceleration and transport processes.

The objective of this research is to use LSK to determine the ion sources and transport processes that led to the distribution functions observed in the *Frank et al.* [1996] studies. In section 2 we introduce Geotail and Wind observations relevant to this study, and in section 3 we outline the methodology used to calculate the magnetic and electric field models and to perform the LSK calculation. In section 4 we discuss the MHD results, compare them to Geotail observations, and show the results of the LSK calculation. We summarize the results and their implications in section 5.

2. OBSERVATIONS

On May 23, 1995, between 0900 UT and 1100 UT the Geotail satellite was located in the near-Earth, near equatorial, magnetotail region (x = -9.5 R_E, y = -3.3 R_E, z = 1.3 R_E in the Earth centered solar-ecliptic (GSE) coordinates we use in this paper). During this time period, the Comprehensive Plasma Instrumentation (CPI) [*Frank et al.*, 1994] onboard the spacecraft observed complex and highly structured ion distribution functions. For the observations presented here the Hot Plasma (HP) analyzer was operated in a mode by which the velocity distributions of ions were determined from more than 3000 samples over the energy-per-unit charge (E/Q) range of 22 V to 48 kV with a repetition rate of 22 s. Plate 1 displays $v_{\parallel}$ versus $v_{\perp}$ for six distribution functions measured by Geotail between 1030 UT and 1036 UT. *Frank et al.* [1996] also published a series of ion velocity distributions measured between 1400 UT and 1406 UT on this day. They concluded from their results that

the distribution functions were nonisotropic. Plate 1 shows the departure of the pitch angle distributions from isotropy with structuring occurring at both high (≥ 500 km/s) and low velocities. Distinct structures in the low energy part of the distribution function can be seen along the $v_\perp = 0$ axis, at $v_{||} = 0$, and at more oblique angles.

During this day the Wind spacecraft was located at $x = 246\ R_E$, $y = 15\ R_E$, and $z = -9\ R_E$. Figure 1 shows the interplanetary magnetic field components, the solar wind velocity, and density measured by Wind and used in the MHD simulation. The input differs from the measurements only in that the values are 3 min averages and that the IMF B_x was held constant at 4 nT. Between 0700 and 1100 UT the IMF B_z component was predominately northward but was interrupted by several small southward turnings. During this time interval, the Wind spacecraft observed a solar wind of unusually high density (~40 cm^{-3}); the solar wind speed and thermal pressure had average values of 350 km/s and 18 pPa, respectively.

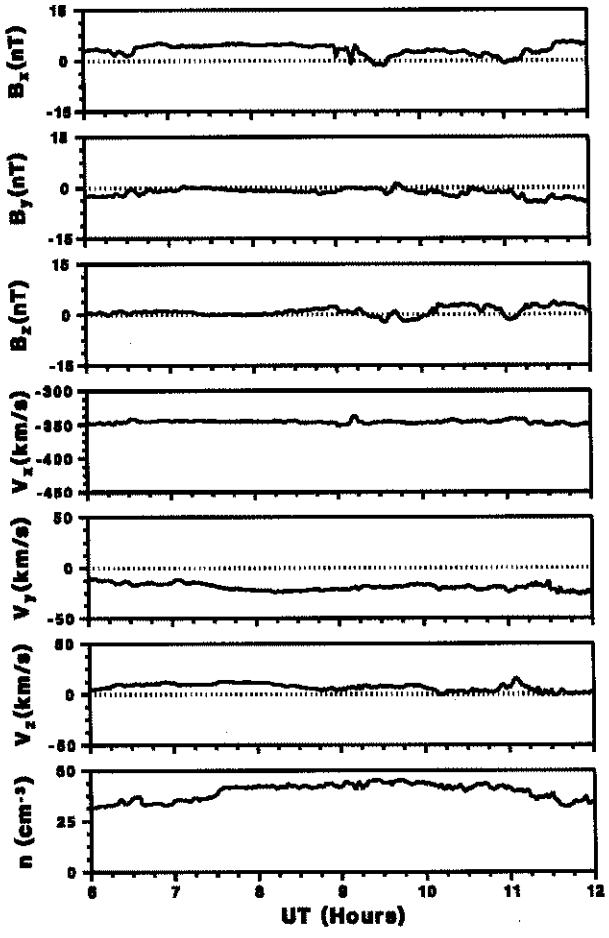

Figure 1. Solar wind parameters for May 23, 1995 from the Wind spacecraft. The figure shows, from top to bottom: the magnetic field components, the velocity components, and the proton density.

3. METHODOLOGY

The understanding of the structures in the chosen distribution function requires an accurate three-dimensional, time-dependent global scale model for the magnetospheric magnetic and electric fields. Currently, such self-consistent fields can be obtained from global MHD simulations alone.

While the three-dimensional, time-dependent magnetic field can be obtained directly from the global MHD simulation, the electric field is calculated from the simulation parameters as:

$$\vec{E} = -\vec{v} \times \vec{B} + \eta\vec{J}$$

where $\vec{v}$ is the bulk flow velocity, $\vec{B}$ is the magnetic field, $\vec{J}$ is the current density, and η is the resistivity. Resistive $\eta\vec{J}$ contributions to $\vec{E}$ become significant only near the magnetopause and near x-lines. The accurate calculation of particle trajectories requires that we use the full electric field, including the resistive term, from the MHD simulation. To investigate the origin of structuring occurring in the distribution functions and the acceleration mechanisms that produced them, the velocity distribution function chosen (lower left panel of Plate 1) is a highly structured one measured by Geotail at 1033:34 UT, when the spacecraft was in the near-Earth plasma sheet ($x = -9.5\ R_E$, $y = -3.3\ R_E$, $z = 1.3\ R_E$). With this distribution function as the starting point for our calculations, we created a numerical distribution function in which f(v) measured by Geotail in each $v_{||}$ - $v_\perp$ bin (50 km/s × 50 km/s) was multiplied by a constant (1.65×10^{27} in this case) to obtain the number of particles in the corresponding bin of the numerical distribution. The particles in each bin are distributed randomly in phase angle; this phase angle randomization was deemed necessary because, in the case of non-adiabatic acceleration, different phase angles can result in different particle trajectories. The resulting distribution function is given in Plate 2, where the color scale denotes the number of particles assigned to a bin. The structuring of the observed distribution is preserved in the numerical distribution function, and this numerical distribution function was assumed in following the trajectories of approximately 90,000 H^+ ions backwards in time from the Geotail location until they reached their "origin," i.e. ei-

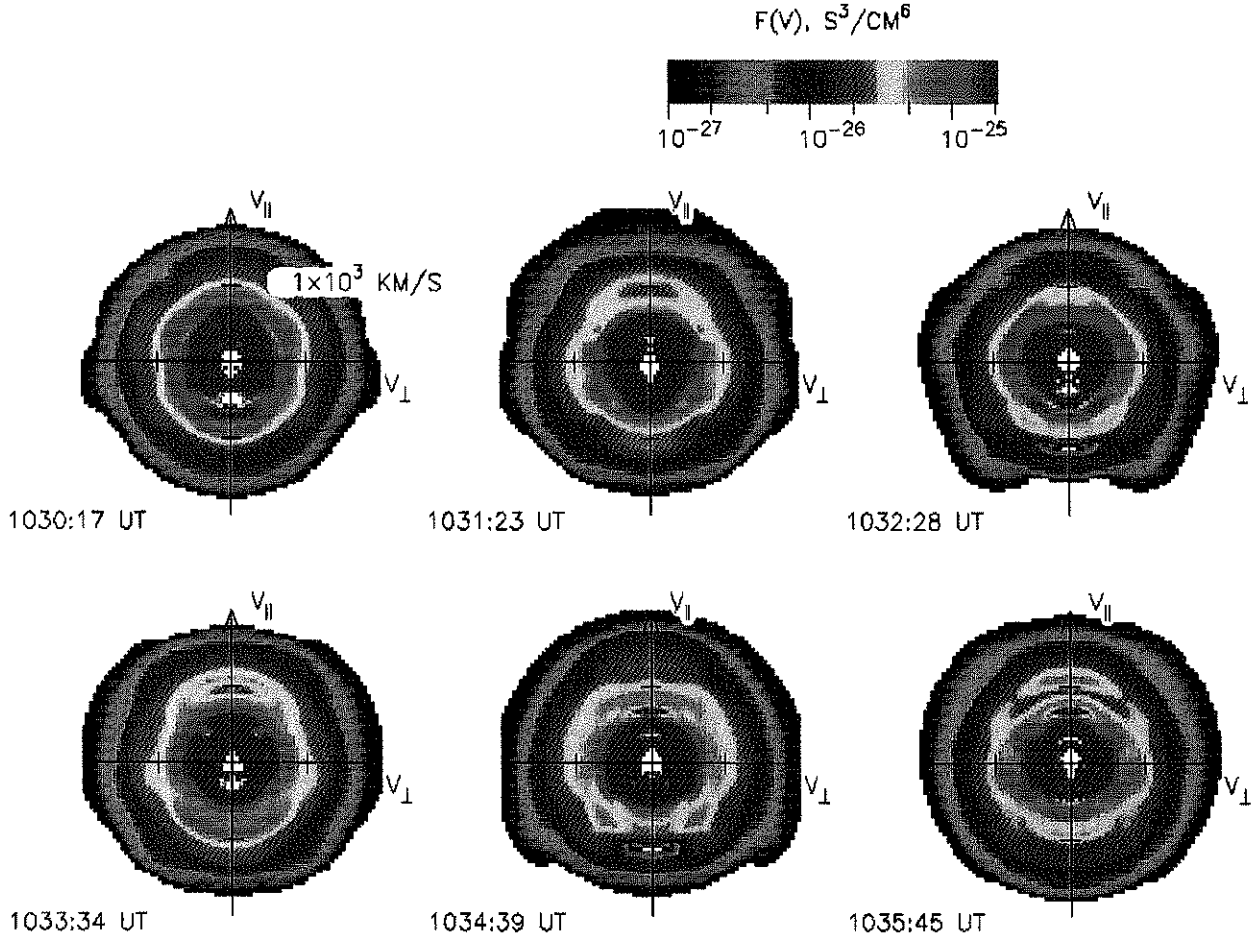

Plate 1. Six pitch angle distribution functions measured by Geotail on May 23, 1995. The phase space densities are color coded according to the bar on top.

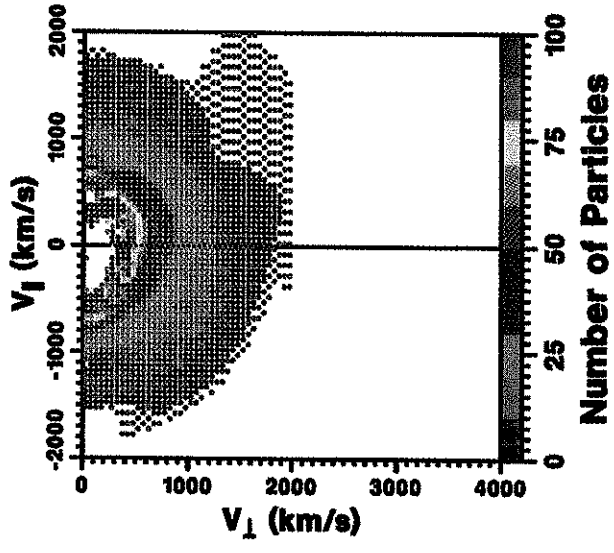

Plate 2. Discretized form of the distribution function measured by Geotail at 1033:34 UT. The color scale on the right gives the number of particles per bin.

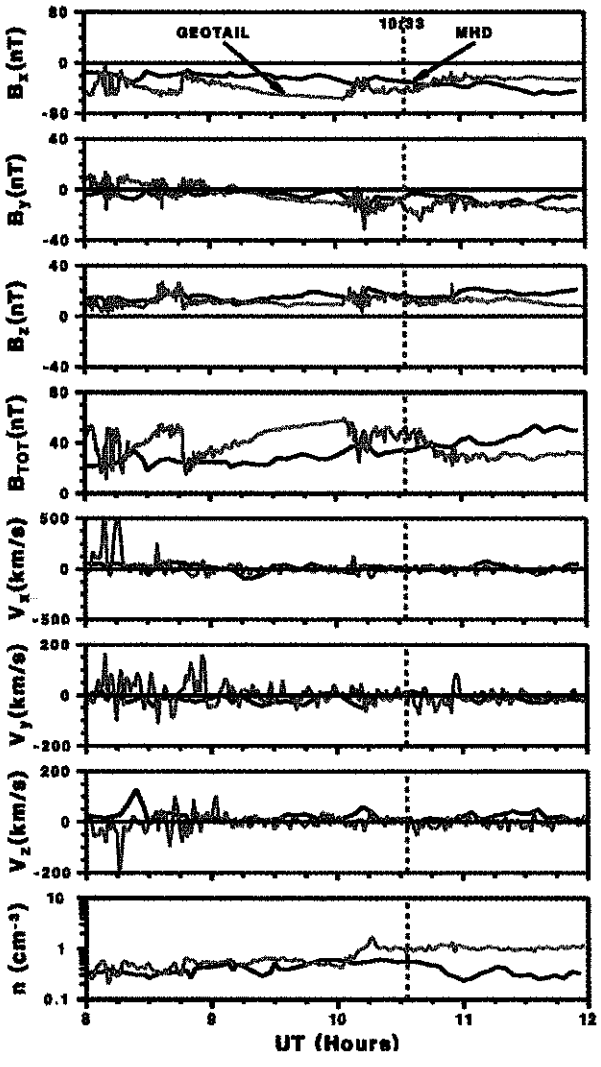

Plate 3. A comparison of time series from Geotail (red curves) and the MHD simulation (black curves). The figure shows, from top to bottom: the magnetic field components, the velocity components, and the proton density.

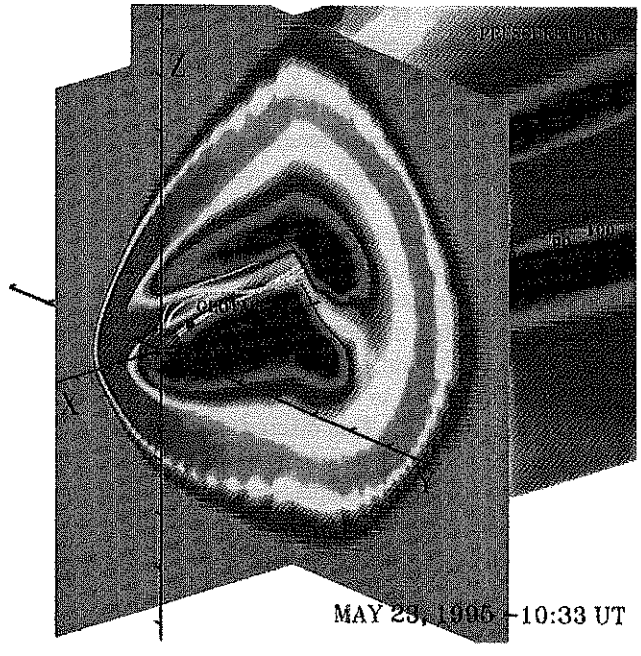

Plate 4. MHD pressure contours at 1033 UT on May 23, 1995, at x = -30 R_E and y = -7 R_E. Field lines showing the existence of an x-line are shown in white.

ther the magnetopause (determined from the MHD fields) or the ionosphere (particles approaching to within 3.7 R_E of the Earth were assumed to originate from the ionosphere).

4. RESULTS

4.1. *MHD results*

As noted above, our study employed the magnetic and electric fields obtained from a global MHD simulation [*Raeder et al.*, 1995] using interplanetary magnetic field (IMF) and plasma data from Wind [*Lepping et al.*, 1995; *Ogilvie et al.*, 1995] as its driving input. The global MHD model results were validated by comparing the time series of the computed parameters with those of the observed density, the bulk flow velocity, and the magnetic field from 0800 UT to 1200 UT. Plate 3 shows the comparison of time series from Geotail with time series from the MHD simulation; the red curves show the Geotail observations. The magnetic field data were obtained from the Geotail MGF experiment [*Kokubun et al.*, 1994] and are shown with 3 s resolution in this figure (top three panels). The plasma data were obtained by using the CPI instrument [*Frank et al.*, 1994] and are shown with 64 s time resolution. During the time interval of interest, 0830 UT to 1040 UT, Geotail was in the southern part of the plasma sheet or its boundary layer. The v_x component of the plasma flow was < 100 km/s and fluctuated between being earthward and tailward streaming (fifth panel). The y and z components of the flow also fluctuated and were small (< 50 km/s) in magnitude (sixth and seventh panels). The density did not show much variation with time and remained near 0.4 cm^{-3} (eighth panel). The time series from the MHD simulation are shown by the black curves. Differences exist between these time series and the Geotail observations. The B_x component from the MHD model is relatively steady with a magnitude of around -25 nT; the observed B_x component, on the other hand, decreased steadily from -25 nT to -50 nT during the time interval 0845 UT to 1000 UT. This discrepancy is a consequence of the fact that Geotail was located in a region of steep gradients, and a small displacement of the spacecraft makes a substantial difference in the results of the MHD model. Also, the dipole orientation is held constant during the simulation run (i.e., to its true orientation at 0800 UT on that day). Thus, we miss the slow drifts in the magnetic field that are due to the wobbling of the Earth's magnetosphere. Because the spacecraft is located on closed field lines at all times, however, these discrepancies should not affect our results.

The B_y and B_z values calculated from the MHD simulation exhibit reasonable quantitative agreement with the measured values (second and third panels from top in Plate 3). The velocity and the density compare fairly well with those from the Geotail observations, except for small scale fluctuations that are probably beyond the capabilities of MHD simulations. As in previous studies [*Frank et al.*, 1995; *Raeder et al.*, 1996, 1997] the time series compared reasonably well and showed the electric and magnetic field model to be gratifyingly realistic.

Plate 4 shows a perspective view of the magnetosphere for 1033 UT that demonstrates the complexity of the magnetosphere during this time period. The two color contours shown in this figure correspond to the pressure from the MHD simulation in the x = -35 R_E and y = -7 R_E planes. The current sheet and the magnetopause, characterized by high pressure, are clearly discernible. The Geotail location around x = -10 R_E is indicated by the black dot. Field lines reflecting the occurrence of reconnection in the MHD model near x = -30 R_E, tailward of Geotail spacecraft, are shown in white in this figure. Reconnection in the tail is a consequence of the successive southward turnings of the IMF observed by the Wind spacecraft on this day.

4.2. *Time dependent LSK results*

The final calculated points of origin for all 90,000 particles are shown in Plate 5. In the upper panel these points are shown projected onto the noon-midnight meridian plane, whereas in the lower panel they are projected onto the equatorial plane. The intersections of the magnetopause with the y = 0 and z = 0 planes are indicated by the solid black curves. The color scale to the right of each panel denotes the number of particles in each 1 R_E × 1 R_E bin. Different sources can be easily identified in Plate 5: (a) the inner (ionospheric) boundary (labeled ionosphere) that supplies more than 40% of the ions at Geotail, (b) the dawn side LLBL located near the equatorial plane ($z \sim 0$) at large y ($\leq$ -15 R_E) and extending between x = -60 R_E and x = -170 R_E, and (c) the plasma mantle extending downtail between x = -25 R_E and x = -140 R_E with entry points appearing at high latitudes near midnight. The next objective was to relate part or all of these sources to specific characteristics of the Geotail distribution function. Plate 6 shows the numerical distribution function with the particles separated according to their origin: Plate 6a shows only the ionospheric ions (35,044 particles or 41% of all ions), Plate 6b shows the LLBL ions (25,576 particles or 31% of all ions), and Plate 6c shows the plasma mantle ions (23,838 particles or 28% of all ions).

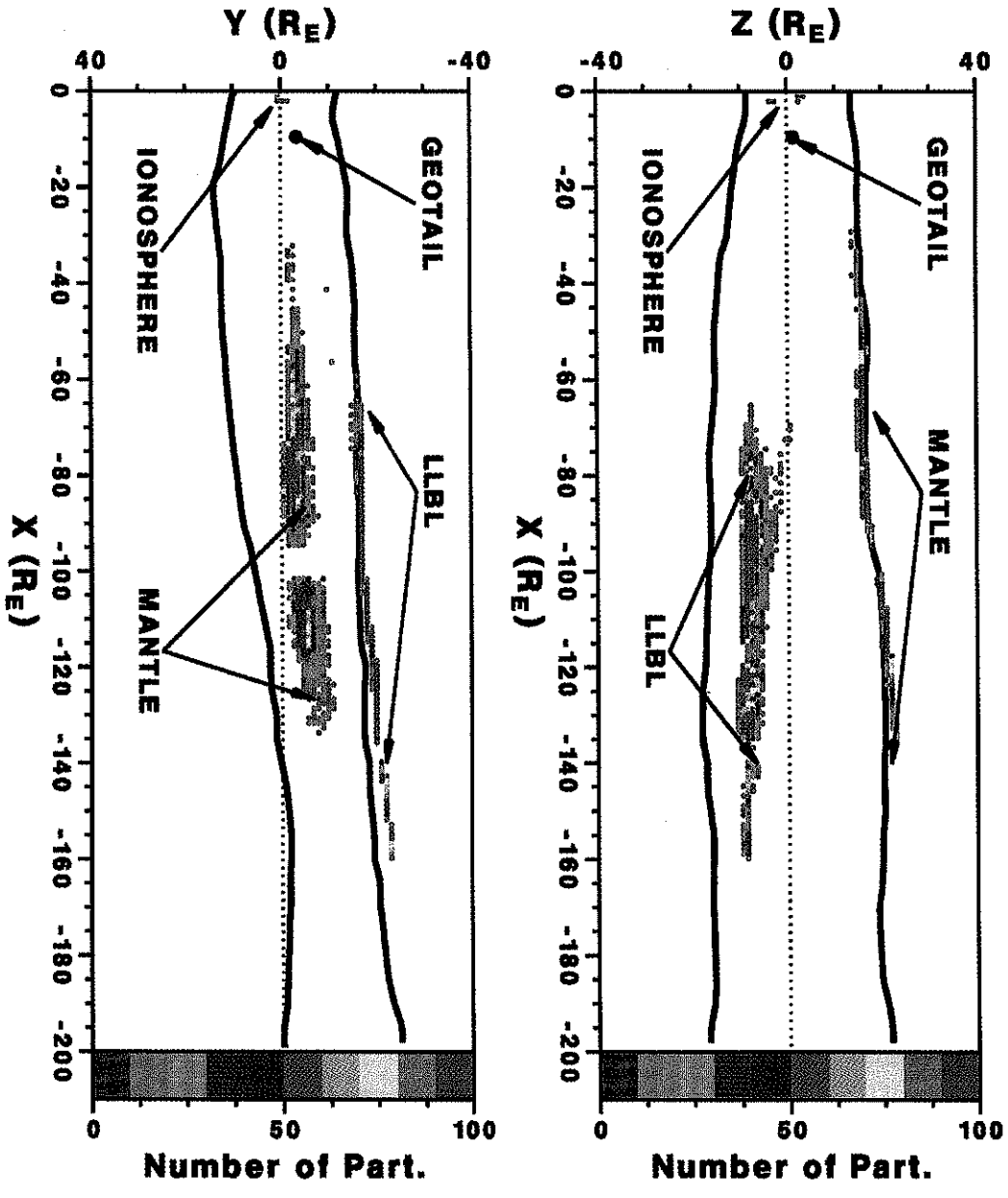

Plate 5. Entry points for ions traced back from the Geotail distribution projected onto (a) the noon-midnight meridional plane and (b) the equatorial plane. The black curves show the location of the intersection of the magnetopause with (a) the y=0 and (b) the z=0 planes. Geotail's location is shown with a large black dot.

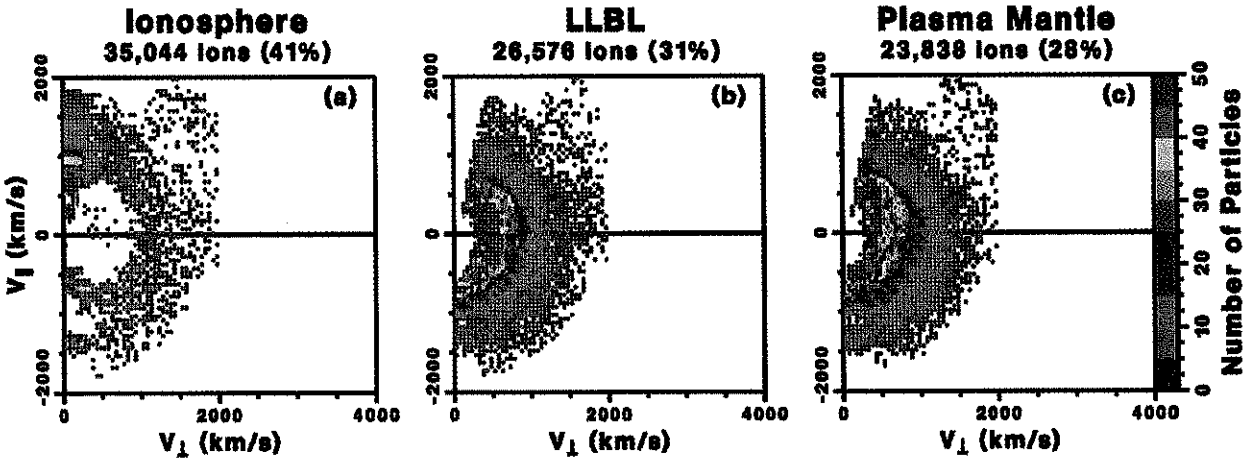

Plate 6. Division of the numerical distribution function (total 90,000 ions) according to the origin of the particles: (a) ionosphere (41% of measured ions), (b) LLBL (31% of ions), and (c) plasma mantle (28% of ions).

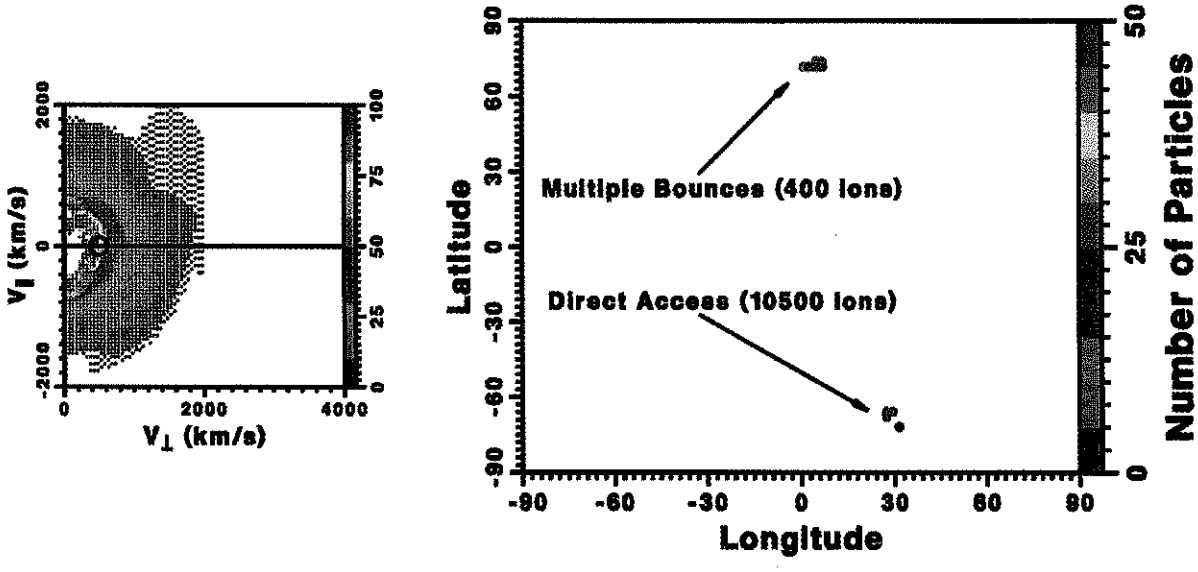

Plate 7. (Left-hand panel) Numerical distribution function with circle showing location of structure at $v_{\perp} \sim 0$ km/s and $v_{\parallel} \sim 300$ km/s. (Right-hand panel) Latitude vs. longitude plot showing origin of ionospheric particles.

4.2.1. *Ionospheric Ions.* More than 40% of the ions observed by Geotail at 1033 UT are of ionospheric origin. Particles from both auroral zones reached the satellite, arriving within < 10° of the field-aligned direction (Plate 6a). A few ionospheric particles were observed with higher pitch angles; these ions had been trapped and mirror bounced before reaching the Geotail location. In order to understand the dynamics of the ionospheric ions measured by Geotail, we examine in detail an individual structure from the Geotail distribution. The left-hand panel of Plate 7 reproduces the numerical distribution function shown in Plate 2 with a circle marking the structure observed at $v_\perp \sim 0$ and $v_\parallel \sim 300$ km/s. Since the ionosphere is the origin of all of the particles in this

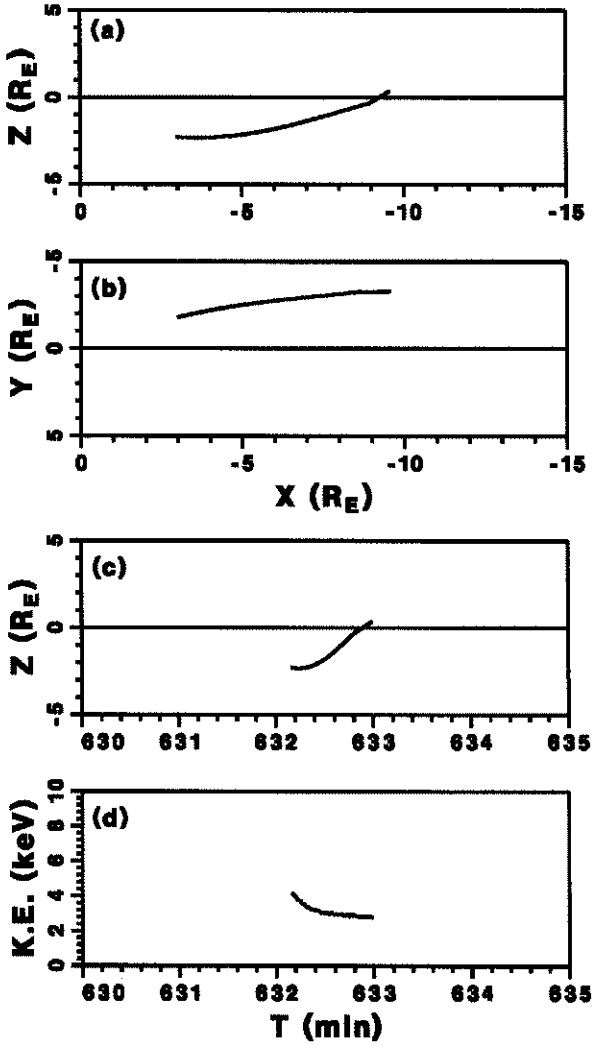

Figure 2. Trajectory of an ionospheric ion having direct access to the Geotail location. The panels show the orbit's projection on the (a) x-z and (b) x-y planes, (c) z versus time, and (d) the particle's kinetic energy versus time.

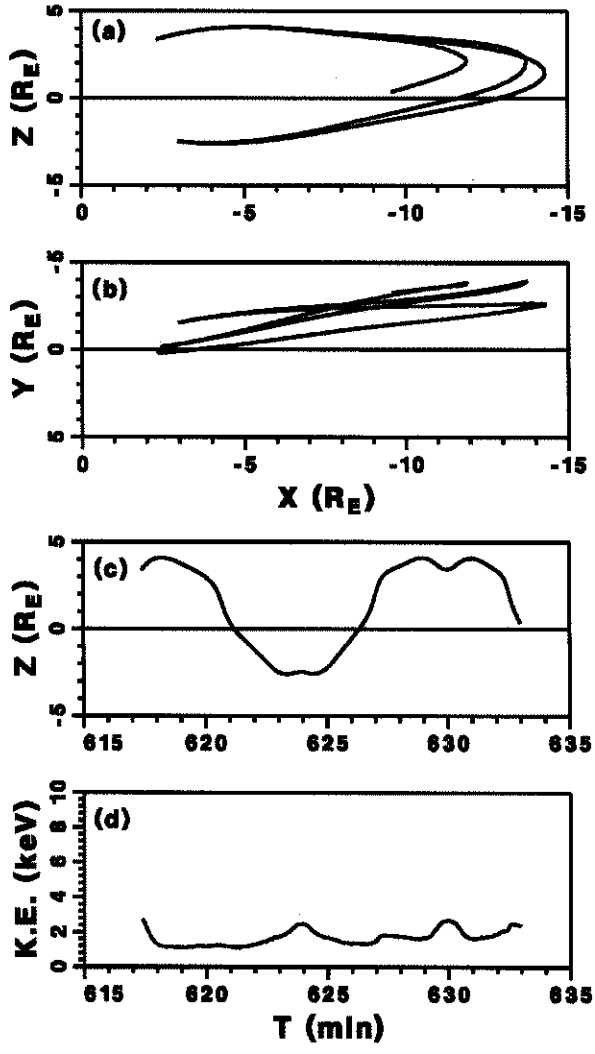

Figure 3. Trajectory of an ionospheric ion reaching Geotail after several bounces, in a format similar to Fig. 2.

structure, the source regions of these ions are shown in a latitude-longitude plot (right hand panel of Plate 7). Two groups of ions can be seen in this figure. The first group, comprised of over 10,000 particles, has direct access to Geotail and arrives at the spacecraft without interacting with the equatorial plane. Figure 2 shows the trajectory of a typical ion from this source. The panel (a) shows the projection of the orbit onto the meridional plane and panel (b) shows the projection of the orbit onto the equatorial plane. Panel (c) shows the particle's z coordinate as a function of time, panel (d) shows the ion's kinetic energy as a function time. This ion spends a very short time in the magnetosphere and arrives at Geotail without any significant change in its kinetic energy. The second group of ions (~ 400 particles) seen in

the right-hand panel of Plate 7 flows out from the northern hemisphere. Ions from this region arrive at Geotail having undergone multiple mirror bounces in the near-Earth magnetotail. Figure 3 depicts a typical particle trajectory from this source region in a format similar to that of Figure 2. The ion crosses the equatorial plane twice before arriving at the spacecraft. Once again, the ion does not gain any energy during its orbit and arrives in the detector field aligned. The source region of both groups of ions in Plate 7 is very localized in latitude (~75° and ~70° in the northern and the southern auroral zones, respectively) and in longitude.

4.2.2. *Low latitude boundary layer ions.* Plate 6b shows that the LLBL contribution to the distribution function is mainly near 90° pitch angle ($v_{||} \sim 0$). We therefore selected a structure observed at $v_{||} \sim 0$ on which to conduct a more detailed analysis. This structure occurs at $v_{\perp} = 500$ km/s and $v_{||} \sim 0$ (indicated by a circle in the left-hand panel of Plate 8). The two right-hand panels of Plate 8 are x - z (upper) and x - y (lower) projections of the magnetotail entry points for particles in this structure and are in a format similar to that of Plate 5. These plots show that the particles responsible for this structure in the Geotail distribution originated in a narrow region extending in x from x = -80 R_E to x = -130 R_E positioned near the low latitude dawn flank of the magnetosphere. Therefore, these particles, which follow guiding center trajectories and are weakly energized, all come from the LLBL.

Figure 4 shows the trajectory of a typical particle from the LLBL source. The format of this figure is similar to that of Figure 2. In order to reveal the nature of this particle's orbit, we have plotted the time history of the κ parameter [*Büchner and Zelenyi*, 1986] for this particle in the lower panel (d) (gray dots, with scale shown on the right of the panel). κ is defined by

$$\kappa \equiv \sqrt{R_c/\rho_L}$$

where R_c is the local magnetic field radius of curvature and ρ_L is the ion Larmor radius. When $\kappa > 1$, particles follow guiding center orbits and are adiabatic. When $\kappa \leq 1$, however, particles no longer conserve their first adiabatic invariant but instead follow stochastic, or quasi-adiabatic, trajectories. The ion shown in Figure 4 enters the magnetosphere in the dawn flank then travels earthward and interacts with the current sheet at $x \sim -28$ R_E and becomes trapped in the near-Earth region; the particle finally reaches Geotail after executing several mirror bounces. Panel (d) of this figure shows that the particle initially has an energy of ~2 keV, which increases to ~4 keV during its first interaction with the current sheet. The increase in energy for this ion is small because κ was ~2 during its current sheet interaction (κ is >> 10 before this interval and is not shown in the figure).

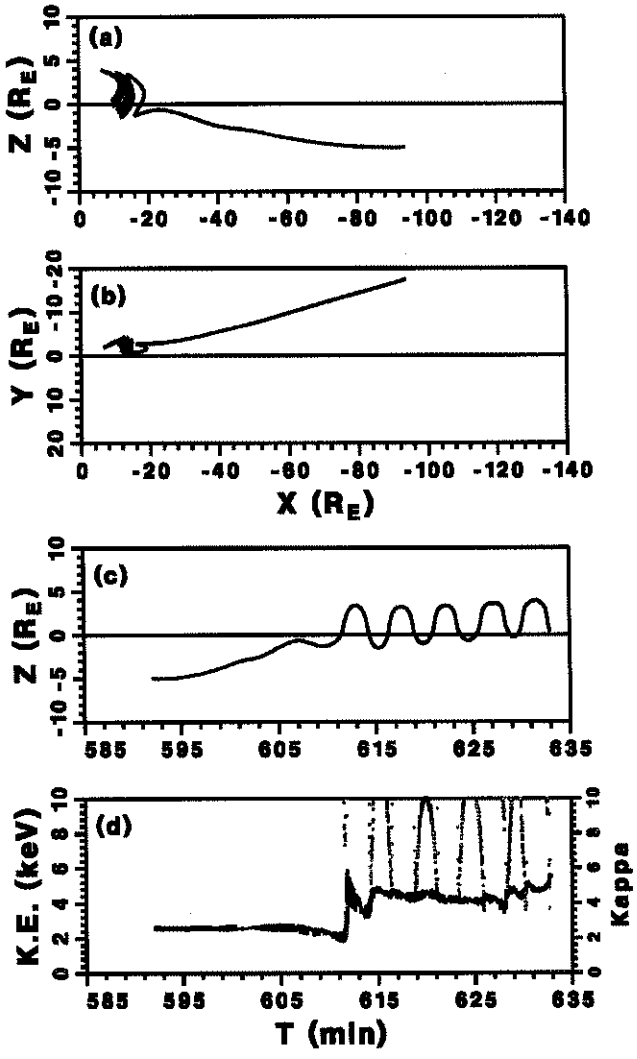

Figure 4. Trajectory of an LLBL ion, in a format similar to Fig. 3. Panel (d) also includes the particle's κ during its orbit (gray dots).

4.2.3. *Plasma mantle ions.* While field aligned particles are mainly ionospheric in origin and the 90° pitch angle particles are from the LLBL, intermediate pitch angle particles with $v_{\perp} \sim 200$ -1000 km/s come from the mantle source, as do ions populating the highest energy part of the distribution. Plate 9 has the same format as Plate 8, but this time the structure is inspected for $v_{\perp} \sim 275$ km/s and $v_{||} \sim 450$ km/s. The right hand panels of

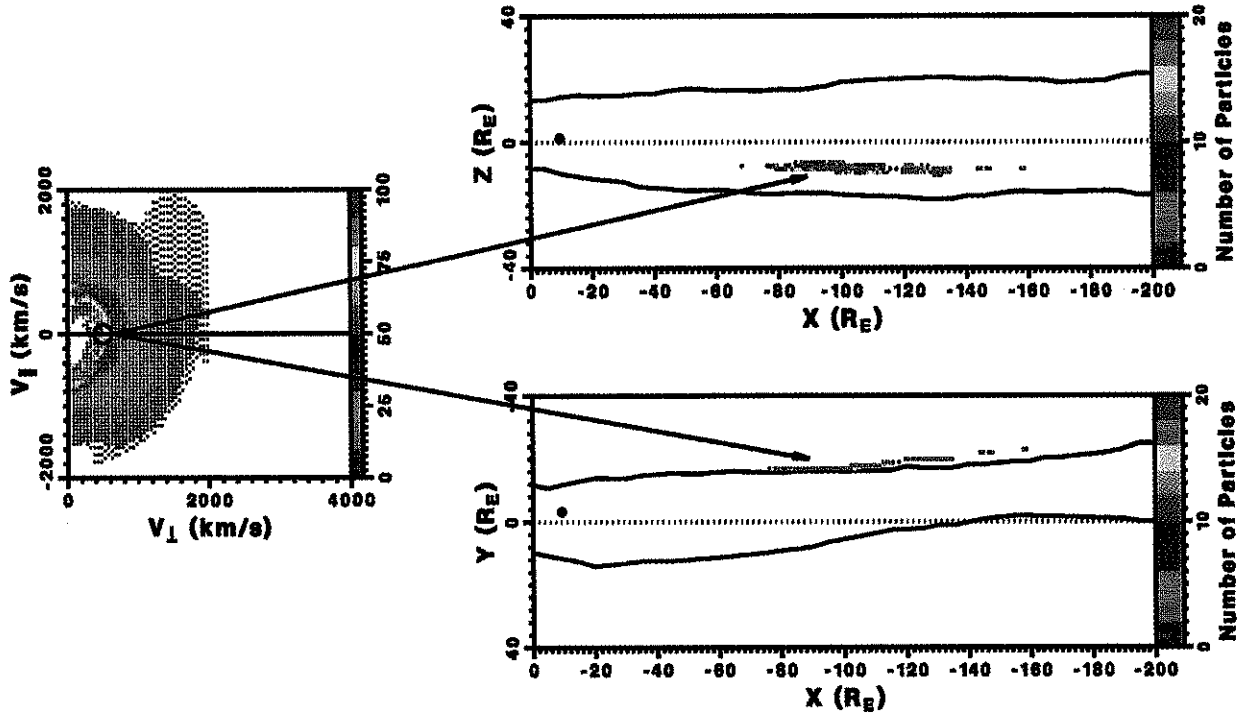

Plate 8. (Left-hand panel) Numerical distribution function with circle showing location of structure at $v_{\perp} \sim 500$ km/s and $v_{\parallel} \sim 0$ km/s. Entry points for all ions in circled structure are projected onto (upper right-hand panel) the noon-midnight meridional plane and (lower right-hand panel) the equatorial plane, in a format similar to Plate 5. Geotail's location is shown with a large black dot.

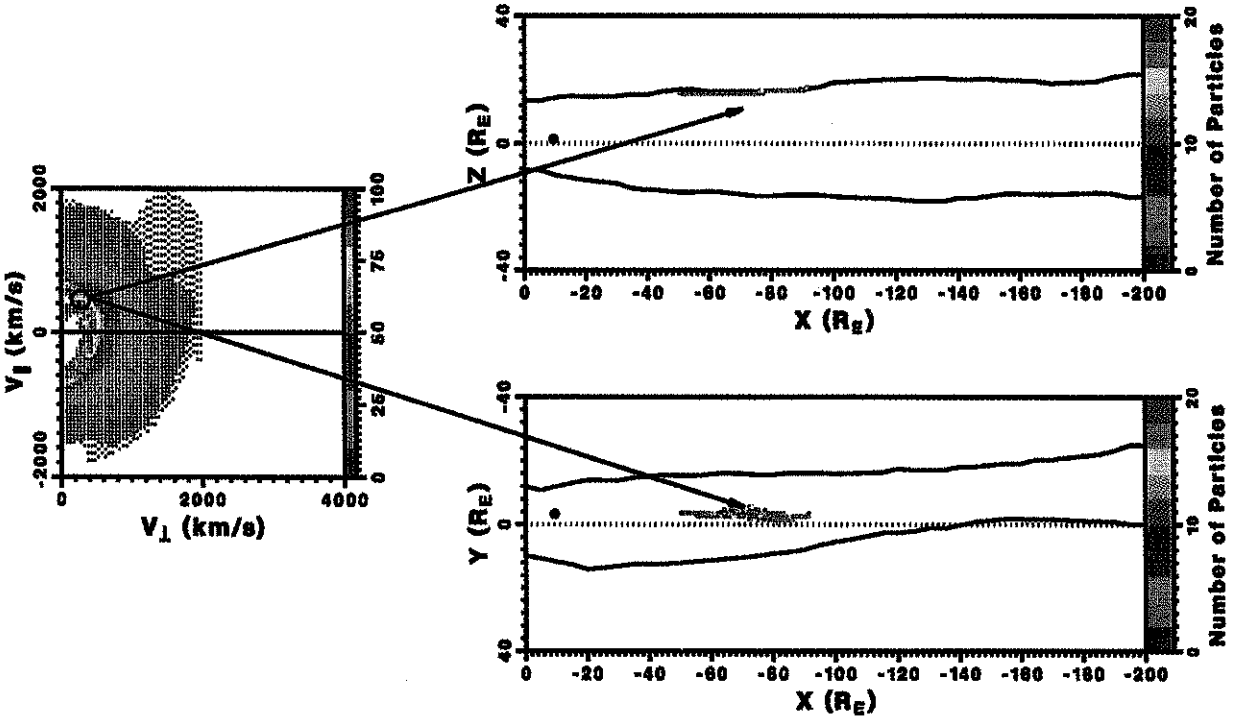

Plate 9. (Left-hand panel) Numerical distribution function with circle showing location of structure at $v_{\perp} \sim 275$ km/s and $v_{\parallel} \sim 450$ km/s. Entry points for all ions in circled structure are projected onto (upper right-hand panel) the noon-midnight meridional plane and (lower right-hand panel) the equatorial plane, in a format similar to Plate 5. Geotail's location is shown with a large black dot.

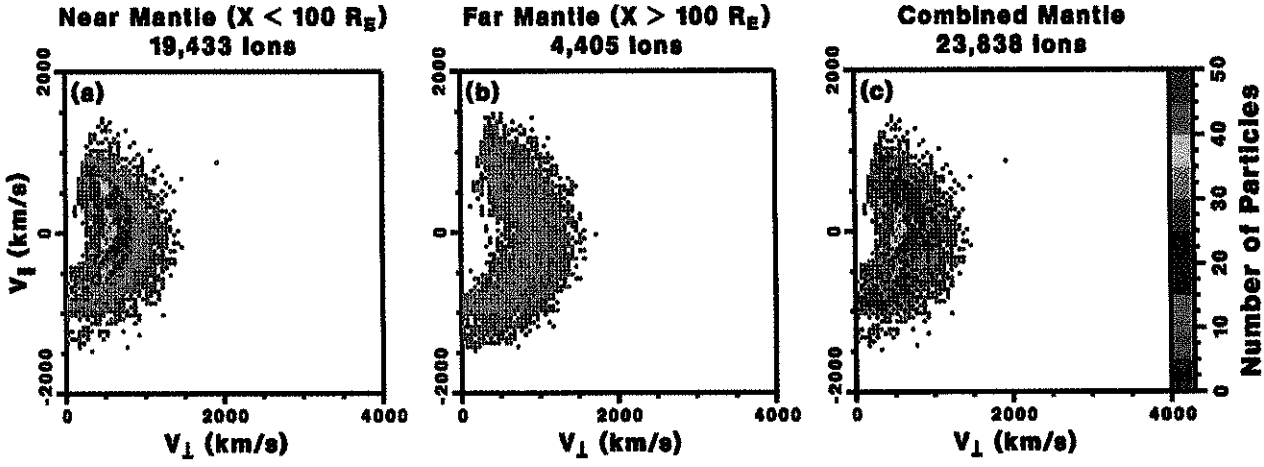

Plate 10. Division of the contribution of mantle ions to the numerical distribution function (total 23,838 ions) into (a) near-Earth mantle ions (19,433 ions), (b) distant mantle ions (4,405 ions), and (c) all mantle ions, with particles from the high-energy structure in the distant mantle source overlaid using black dots.

Plate 9 show that the ions in this structure originated in a narrow high latitude region ($y \sim 0$, $z \geq 18\ R_E$) and a region in x where $-85\ R_E < x < -55\ R_E$.

Figure 5 shows a particle trajectory typical of the near-Earth ($x \geq -90\ R_E$) portion of the plasma mantle. The ion depicted enters the magnetotail at $x \sim -80\ R_E$, convects earthward and is trapped in the near-Earth region without interacting with the current sheet. The κ for this particle remains high ($\kappa > 4$, with $\kappa >> 10$ for most of the orbit) and the ion is only weakly energized during its orbit. Plate 9 indicates that only a small portion of the near-Earth plasma mantle source has contributed ions to the structure at $v_\perp \sim 275$ km/s and $v_\parallel \sim 450$ km/s. To reach a better understanding of the role of mantle ions arriving from the distant tail, we plot in Figure 6 the trajectory of a mantle ion originating from $x \sim -110\ R_E$. In contrast to the ion from the near-Earth mantle source, this particle undergoes several nonadiabatic interactions with the current sheet at $x \sim -25\ R_E$ and is quickly energized to ~ 10 keV. Note that $\kappa < 1$ for the period when the ion gains most of its energy (gray dots in panel (d) of Figure 6). Thus, ions from the distant tail mantle source arrive at Geotail with higher energies than particles originating from the near-Earth mantle source. This point is illustrated in Plate 10, in which we have separated the contribution of the plasma mantle source to the Geotail distribution into two portions: that from the near-Earth mantle ($x \geq -100\ R_E$, Plate 10a), and that from the distant mantle ($x < -100\ R_E$, Plate 10b). The peak of the distribution from the near-Earth mantle occurs at $v_\parallel = 500$ km/s, while the much smaller peak in the distant tail mantle ion distribution occurs at $v \sim 1000$ km/s. This is also illustrated in Plate 10c, where we have superposed the distant tail mantle peak (shown with black dots) onto the combined mantle distribution. Plate 10c unambiguously illustrates that the two mantle sources are responsible for populating distinct regions of phase space.

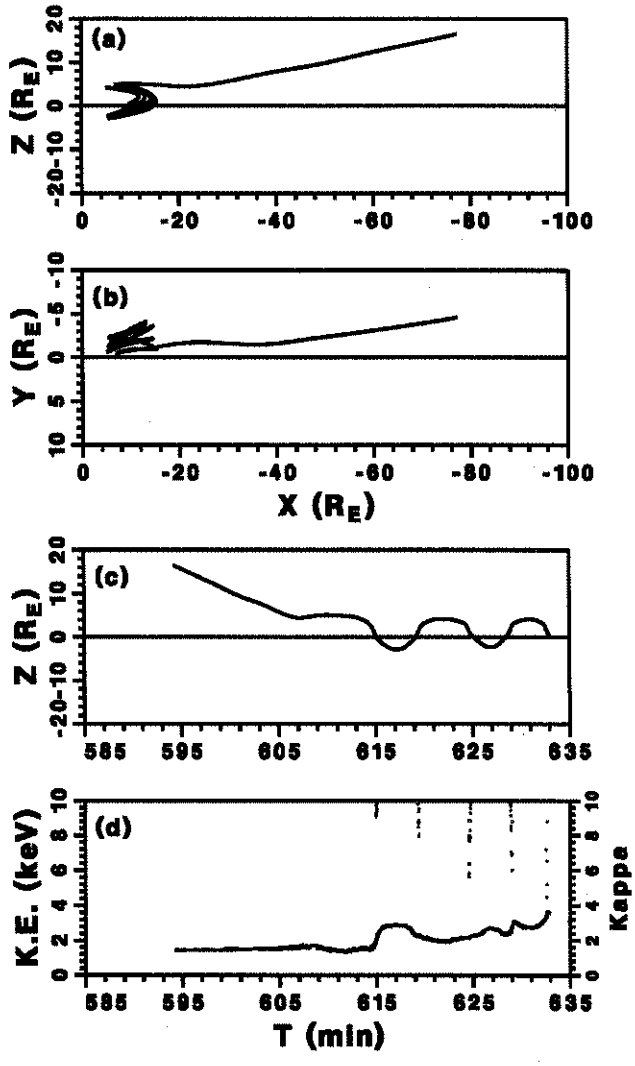

Figure 5. Trajectory of a particle originating in the near-Earth plasma mantle, in a format similar to Fig. 4.

5. DISCUSSION AND CONCLUSIONS

In this paper we have presented a detailed analysis of an observed Geotail distribution function based on a combination of MHD and LSK techniques. A virtual satellite was placed in an MHD electric and magnetic field model at the position of the Geotail satellite at the time of the observation. The MHD simulation was based on solar wind conditions observed by the Wind spacecraft. A structured distribution function observed at Geotail provided the velocity space distribution for launching time-reversed ions in the MHD model. Plasma mantle, LLBL and ionospheric sources all contributed to this distribution function. While the majority of the particles arrived at the Geotail position through adiabatic processes the highest energy ions were influenced by nonadiabatic acceleration at the current sheet. The specific sources and transport histories of individual structures were identified.

Just as we checked on the validity of the MHD model it is advisable to consider the reliability of the particle trajectory results. Because the initial distribution function was based on the Geotail distribution we clearly must reproduce this distribution. Unfortunately, the particle trajectory results cannot be compared with observations as easily as the MHD result could. However, there

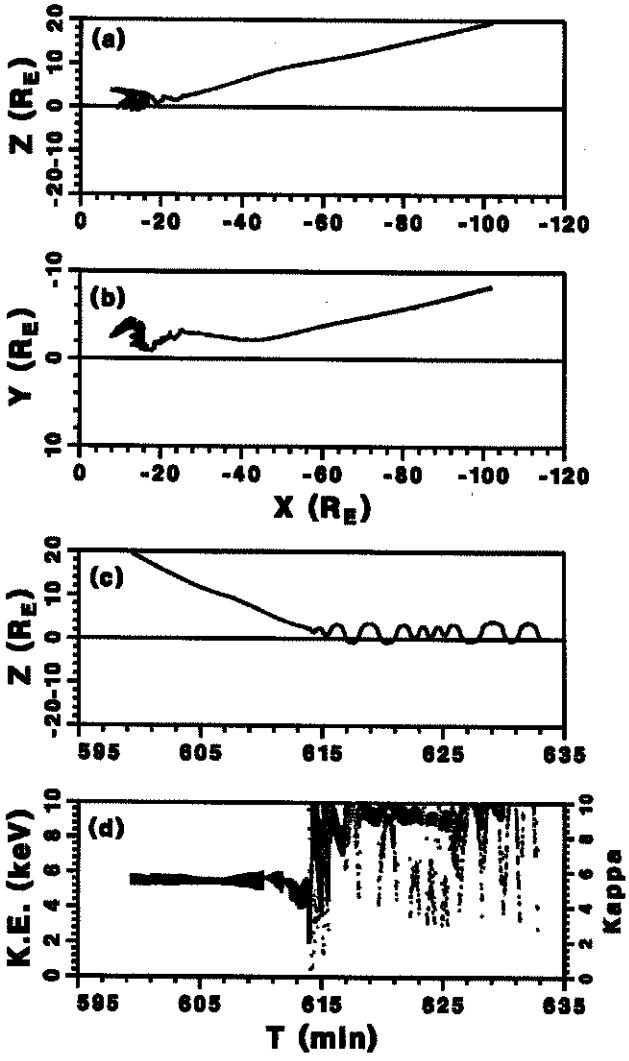

Figure 6. Trajectory of a particle originating in the distant plasma mantle, in a format similar to Fig. 4.

are two features of the results that give us confidence in them. One is that the inferred sources are consistent with well established sources of magnetospheric protons (ionosphere, LLBL and plasma mantle) that could all reasonably be active under the observed IMF conditions. A second is the strong correspondence of individual structures in the distribution with individual sources. While any point in phase space could be mapped to a source location by the methods we employed and any distribution could than be divided up among various sources, a "bump" on the observed distribution in a region of phase space mapping to an actual magnetospheric source, say, the plasma mantle would not be expected if this association were random.

Another interesting feature of the results is that, in spite of non-adiabatic or multiple encounters with the current sheet, the particles are seen to originate from relatively narrow regions on the magnetopause, indicating that the transport process is not diffusive in the sense that it does not seem to destroy information about the source locations of the particles' origin, a promising result for this type of calculation. This result also confirms previous model calculations [*Ashour-Abdalla et al.*, 1996] that indicate non-adiabatic processes contribute to the production of higher energy ions in the plasma sheet, especially for a plasma mantle source whose ions interact with the weak field in the distant tail. Furthermore, note that while MHD simulations would trace the origin of a parcel of fluid at a location within the magnetosphere to a single source location, our calculation shows that multiple sources can contribute to a given observed distribution. This shows that, though the validity of MHD results have been confirmed in general, LSK calculations are required to explain distribution functions in detail, at least for certain conditions. The ions reflect the past history of the magnetotail configuration that in turn reflects the past history of the solar wind.

The backwards tracing of particles in the magnetosphere is currently limited by the failure of the model in the extremely sharp gradients near the magnetopause (which is the reason for stopping the particles before they reach this region). The sources that we determine in this calculation may be influenced by processes occurring prior to entry that we cannot capture. For example, *Richard et al.* [1994] showed that LLBL particles could originate at the cusp reconnection region. Ultimately it would be a great benefit to space weather prediction (as well as to a general understanding of magnetospheric physics) if particles could be run forward in time from the solar wind and ionosphere and distribution functions obtained everywhere in the magnetosphere, but this would require vast numbers of particles. Currently our method seems to be the only tractable one that can resolve the full details of a local distribution function.

Acknowledgments. This work was supported by NASA grants NAG5-1100, NAGW-4553. Computing support was provided by the Maui High Performance Computing Center, the Office of Academic Computing at UCLA, the San Diego Supercomputer Center, and the Cornell Theory Center. UCLA/IGPP publication number 4939.

REFERENCES

Amano, K., and T. Tsuda, Particle trajectories at a neutral point, *J. Geomag. Geoelect., 30*, 7, 1978.

Ashour-Abdalla, M., J. Berchem, J. Büchner, and L. Zelenyi, Shaping of the magnetotail from the mantle: Global and local structuring, *J. Geophys. Res.*, *98*, 5651, 1993.

Ashour-Abdalla, M., L. M. Zelenyi, V. Peroomian, and R. L. Richard, Consequences of magnetotail ion dynamics, *J. Geophys. Res.*, *99*, 14,891, 1994.

Ashour-Abdalla, M., L. M. Zelenyi, V. Peroomian, R. L. Richard, and J. M. Bosqued, The mosaic structure of plasma bulk flows in the Earth's magnetotail, *J. Geophys. Res.*, *100*, 19,191, 1995.

Ashour-Abdalla, M., L. A. Frank, W. R. Paterson, V. Peroomian, and L. M. Zelenyi, Proton velocity distributions in the magnetotail: Theory and observations, *J. Geophys. Res.*, *101*, 2587, 1996.

Balsiger, H., P. Eberhardt, J. Geiss, and D. T. Young, Magnetic storm injection of 0.9 - 16 keV/e solar and terrestrial ions into the high-altitude magnetosphere, *J. Geophys. Res.*, *85*, 1645, 1980.

Büchner, J., and L. M. Zelenyi, Deterministic chaos in the dynamics of charged particles near a magnetic field reversal, *Phys. Lett. A*, *118*, 395, 1986.

Büchner, J., and L. M. Zelenyi, Regular and chaotic charged particle motion in magnetotail-like field reversals, 1. Basic theory of trapped motion, *J. Geophys. Res.*, *94*, 11821, 1989.

Chen, J., and P. J. Palmadesso, Chaos and nonlinear dynamics of single particle orbits in a magnetotail-like magnetic field, *J. Geophys. Res.*, *91*, 1499, 1986.

Cowley, S. W. H., Plasma populations in a simple open model magnetosphere, *Space Sci. Rev.*, *26*, 217, 1980.

Curran, D., and C. K. Goertz, Particle distributions in a two-dimensional reconnection field geometry, *J. Geophys. Res.*, *94*, 272, 1989.

Eastman, T. E., and E. W. Hones, Characteristics of the magnetospheric boundary layer and magnetopause layer as observed by IMP 6, *J. Geophys. Res.*, *84*, 2019, 1979.

Eastman, T. E., E. W. Hones, S. J. Bame, and J. R. Asbridge, The magnetospheric boundary layer: Site of plasma, momentum and energy transfer from the magnetosheath into the magnetosphere, *Geophys. Res. Lett.*, *3*, 685, 1976.

Frank, L. A., K. L. Ackerson, W. R. Paterson, J. A. Lee, M. R. English, and G. L. Pickett, The Comprehensive Plasma Instrumentation (CPI) for the GEOTAIL spacecraft, *J. Geomagn. Geoelec.*, *46*, 23, 1994.

Frank, L. A., M. Ashour-Abdalla, J. Berchem, J. Raeder, W. R. Paterson, S. Kokubun, T. Yamamoto, R. P. Lepping, F. V. Coroniti, D. H. Fairfield, and K. L. Ackerson, Observations of plasmas and magnetic fields in Earth's distant magnetotail: Comparison with a global MHD model, *J. Geophys. Res.*, *100*, 19177, 1995.

Frank, L. A., W. R. Paterson, K. L. Ackerson, S. Kokubun, and T. Yamamoto, The Plasma velocity distributions in the near-Earth plasma sheet: A first look with the Geotail spacecraft, *J. Geophys. Res.*, *101*, 10627, 1996.

Geiss, J., H. Balsiger, P. Eberhardt, H. P. Walker, L. Weber, D. T. Young, and H. Rosenbauer, Dynamics of magnetospheric ion composition as observed by the Geos mass spectrometer, *Space Sci. Rev.*, *22*, 537, 1978.

Green, J. L., and J. L. Horwitz, Destiny of earthward streaming plasma in the plasma sheet boundary layer, *Geophys. Res. Lett.*, *13*, 76, 1986.

Hill, T. W., Origin of the plasma sheet, *Rev. of Geophys. and Space Phys.*, *12*, 379, 1974.

Hones, E. W., S.-I. Akasofu, S. J. Bame, M. D. Montgomery, S. Singer, and S.-I. Akasofu, Measurements of magnetotail plasma flow made with Vela 4B, *J. Geophys. Res.*, *77*, 5503, 1972*a*.

Hones, E. W., S.-I. Akasofu, S. J. Bame, and S. Singer, Outflow of plasma from magnetotail into the magnetosheath, *J. Geophys. Res.*, *77*, 6688, 1972*b*.

Jaeger, E. F., and T. W. Speiser, Energy and pitch angle distributions for auroral ions using the current sheet acceleration model, *Adv. Space Res.*, *28*, 129, 1974.

Kokubun, S., T. Yamamoto, M. H. Acuna, K. Hayashi, K. Shiokawa, and H. Kawano, The GEOTAIL magnetic field experiment, *J. Geomag. Geoelec.*, *46*, 7, 1994.

Lennartsson, W., E. G. Shelley, R. D. Sharp, R. G. Johnson, and H. Balsiger, Some initial ISEE-1 results on the ring composition and dynamics during the magnetic storm of December 11, 1977, *Geophys. Res. Lett.*, *6*, 483, 1979.

Lennartsson, W., R. D. Sharp, E. G. Shelley, R. G. Johnson, and H. Balsiger, Ion composition and energy distribution during 10 magnetic storms, *J. Geophys. Res.*, *86*, 4678, 1981.

Lepping, R. P., et al., The Wind Magnetic Field Investigation, *Space Sci. Rev.*, *71*, 207, 1995.

Lundin, R., L. R. Lyons, and N. Pissarenko, Observations of the ring current composition at L < 4, *Geophys. Res. Lett.*, *7*, 425, 1980.

Lyons, L. R., and T. W. Speiser, Evidence for current-sheet acceleration in the geomagnetic tail, *J. Geophys. Res.*, *87*, 2276, 1982.

Martin, R. F., Chaotic particle dynamics near a two-dimensional magnetic neutral point with application to the geomagnetic tail, *J. Geophys. Res.*, *91*, 985, 1986.

Martin, R. F., and T. W. Speiser, A predicted energetic ions signature of a neutral line in the geomagnetic tail, *J. Geophys. Res.*, *93*, 11,521, 1988.

Ogilvie, K. W., et al., SWE, A comprehensive plasma instrument for the Wind spacecraft, *Space Sci. Rev.*, *71*, 55, 1995.

Pilipp, W. G., and G. Morfill, The formation of the plasma sheet resulting from plasma mantle dynamics, *J. Geophys. Res.*, *83*, 5670, 1978.

Raeder, J., R. J. Walker, and M. Ashour-Abdalla, The structure of the distant geomagnetic tail during long periods of northward IMF, *Geophys. Res. Lett.*, *22*, 349, 1995.

Raeder, J., J. Berchem, and M. Ashour-Abdalla, The importance of small scale processes in global MHD simulations: Some numerical experiments, in *The Physics of Space Plasmas*, edited by T. Chang and J. R. Jasperse, *14*, MIT Center for Theoretical Geo/Cosmo Plasma Physics, Cambridge, MA, 403, 1996.

Raeder, J., J. Berchem, M. Ashour-Abdalla, L. A. Frank, W. R. Paterson, K. L. Ackerson, R. P. Lepping, K. Ogilvie, S. Kokubun, T. Yamamoto, and D. Fairfield, The distant tail under strong northward IMF conditions: Global MHD results for the Geotail March 29, 1993 observations, *J. Geophys. Res.*, submitted, 1997.

Richard, R. L., R. J. Walker, and M. Ashour-Abdalla, The population of the magnetosphere by solar wind ions when the interplanetary magnetic field is northward, *Geophys. Res. Lett.*, *21*, 2455, 1994

Savenkov, B. V., L. M. Zelenyi, M. Ashour-Abdalla, and J. Büchner, Regular and chaotic aspects of charged particle motion in a magnetotail-like field with a neutral line, *Geophys. Res. Lett.*, *18*, 1587, 1991.

Schindler, K., and J. Birn, On the generation of field-aligned plasma flow at the boundary of the plasma sheet, *J. Geophys. Res.*, *92*, 95, 1987.

Sharp, R. D., D. L. Carr, W. K. Peterson, and E. G. Shelley, Ion streams in the magnetotail, *J. Geophys. Res.*, *86*, 4639, 1981.

Shelley, E. G., R. G. Johnson, and R. D. Sharp, Satellite observations of energetic heavy ions during a geomagnetic storm, *J. Geophys. Res.*, *77*, 6104, 1972.

Speiser, T. W., Particle trajectories in a model current sheet based on the open model of magnetosphere, with applications to auroral particles, *J. Geophys. Res.*, *70*, 4216, 1965.

Tsyganenko, N. A., A magnetospheric magnetic field model with a warped tail current sheet, *Planet. Space Sci.*, *37*, 5, 1989.

Wagner, J. S., P. C. Gray, J. R. Kan, T. Tajima, and S.-I. Akasofu, Particle dynamics in reconnection field configurations, *Planet. Space Sci*, *29*, 391, 1981.

Williams, D. J., Energetic ion beams at the edge of the plasma sheet: ISEE 1 observations plus a simple explanatory model, *J. Geophys. Res.*, *86*, 5501, 1981.

Zelenyi, L. M., J. Büchner, and D. V. Zogin, Quasiadiabatic ion acceleration in the Earth's magnetotail, *Proceedings of Varenne-Abustuman Workshop on Plasma Astrophysics*, Eur. Space Agency Spec. Publ., ESA-SP285, 1988.

Maha Ashour-Abdalla, Mostafa El-Alaoui, Vahé Peroomian, Joachim Raeder, Robert L. Richard, and Ray J. Walker, Institute of Geophysics and Planetary Physics, University of California, Los Angeles, CA 90095-1567 (e-mail mabdalla@igpp.ucla.edu).

Lev M. Zelenyi, Space Research Institute, Russian Academy of Sciences, 117810 Moscow, Russia.

L. A. Frank, and W. R. Paterson, Department of Physics and Astronomy, The University of Iowa, Iowa City, IA 52242.

J. M. Bosqued, Centre d'Etude Spatiale des Rayonnements, CNRS, BP 4346, 31029 Toulouse Cedex, France.

R. P. Lepping, and K. Ogilvie, NASA/Goddard Space Flight Center, Greenbelt, MD 20771.

S. Kokubun, STELAB, Nagoya University, Toyokawa, Aichi 442, Japan.

T. Yamamoto, ISAS, Sagamihara, Kanagawa 229, Japan.